Journal of Energy Storage 134 (2025) 118080

Contents lists available at ScienceDirect

Journal of Energy Storage

journal homepage: www.elsevier.com/locate/est

Research papers

A hierarchical multi-objective co-optimization for capacity design and control strategy of PV air conditioning coupled with load flexibility and batteries

Sihui Li [a], Yonghuan Li [a], Meng Wang [a,*], Li Xie [a], Guowei Bo [a], Chujie Lu [b]

[a] College of Energy and Power Engineering, Changsha University of Science and Technology, Changsha 410114, PR China
[b] Faculty of Architecture and the Built Environment, Delft University of Technology, the Netherlands

ARTICLE INFO

Keywords:
Photovoltaic direct-driven air conditioning
Energy control strategy
Economic feasibility
Environmental sustainability
Load flexibility

ABSTRACT

Proper co-optimization of photovoltaic driven air conditioning (PVAC) systems with load flexibility and batteries is pivotal for achieving zero energy buildings (ZEBs). However, practical implementation faces challenges from separate optimization with conflicting objectives, neglect of spatial-temporal occupancy features, and limited consideration of energy, economic, and environmental performance. This study proposes a hierarchical multi-objective co-optimization framework for capacity design and control strategy of the PVAC coupling systems, with the two optimization layers sharing the same multi-objective function. The optimization method balances energy, economic, environmental performance by key metrics including thermal comfort satisfaction ratio (TCSR), grid cumulative action power (GP_{total}), net present value (NPV) and emission reduction (ER). The optimal capacity optimization of PV and batteries for PVAC systems was solved by the NSGA-II and TOPSIS algorithms. Based on the case study of a multi-functional academic building, the optimization results of the off-grid system and the grid-connected system were calculated under different configuration of PV and battery capacity, and the relationship between the indicators was discussed. The optimization method of off-grid PVAC systems achieves 24 % reduction in PV capacity while maintaining 85.85 % TCSR, 123,800 CNY of NPV, and 167.26 tons of ER. Grid-connected systems with 165.88 kW PV capacity and 71.26 kWh battery capacity can achieve 100 % of TCSR, 1861.8 kW of GP_{total}, 148,300 CNY of NPV, and 174.70 tons of ER. The study provides an innovative and practical method for capacity design and energy control of PVAC coupling systems to achieve zero energy buildings.

1. Introduction

1.1. Background

The United Nations Sustainable Development Goals (SDGs) mandate a 40 % reduction in building sector carbon emissions by 2030 [1,2]. The building currently accounts for approximately 33 % of global energy consumption and 40 % of global carbon emissions, with both trends exhibiting persistent upward trajectories [3,4]. With this sector, heating, ventilation, and air conditioning (HVAC) systems constitute over 40 % of energy use [5,6], presenting significant challenges for achieving carbon neutrality objectives and zero energy buildings. Photovoltaic-driven air conditioning (PVAC) systems offer a promising solution by leveraging the consistency between PV generation and AC energy consumption to reduce grid dependency, primary energy consumption, and associated emissions [7,8].

Despite these advantages, PVAC systems face some practical barriers [9,10]. Energy mismatching issues frequently arise from fluctuating PV generation and variable AC energy consumption, highlighting the need to optimize system design and energy control. PVAC design optimization includes increasing PV capacity, integrating energy storage devices, and leveraging AC load flexibility [11,12]. However, the design of the PVAC coupling system is complex, as it involves many parameters related to PV, AC units, batteries, and buildings. This complexity hinders achieving optimal energy performance. Moreover, energy control strategies (e.g., load flexibility management, PV generation adjustment, and battery power dispatch) are constrained by system design parameters, causing a co-optimization of capacity and control strategy for PVAC coupling

* Corresponding author.
E-mail address: wangmeng@csust.edu.cn (M. Wang).

https://doi.org/10.1016/j.est.2025.118080
Received 14 April 2025; Received in revised form 16 July 2025; Accepted 12 August 2025
Available online 19 August 2025

systems [14,15].

Existing research on PVAC systems mainly focuses on optimizing either system capacity or control strategies under specific configurations [13]. However, the comprehensive optimization for capacity design and control strategy is crucial for practical applications. Additionally, existing studies often prioritize energy performance while overlooking the impacts on carbon emissions and economic efficiency [16]. A systematic analysis of PVAC coupling system optimization for both capacity design and control strategy under multi-objective considerations of energy, economic, and environmental performance is worth noting.

1.2. Related work on optimization technologies for PVAC systems

Extensive research has been conducted on improving the energy performance of PVAC by using different optimization technologies [10]. Owing to the good consistency between PV generation and AC energy consumption, along with technological advancements and price advantages of PV products, increasing PV capacity has become a common method for enhancing energy matching of PVAC systems [17]. Zhao et al. suggested that the optimal PV capacity of office buildings should cover the total AC consumption [18]. However, Li et al. noted that intermittent PV generation restricts energy matching across different time scales and climatic zones, reducing the effectiveness of simply increasing PV capacity [19,20]. Moreover, rapid increases in PV capacity exacerbate real-time energy mismatches, imposing significant grid operational stress.

Batteries are widely used to mitigate real-time fluctuations in PV generation and ensure reliable operation [21]. Opoku et al. [23] demonstrated that battery integration can increase the average solar energy utilization rate to 60 %. To further improve the energy matching across different climate zones, Ozcan et al. [24] found that the annual SC and SS of the system equipped with a 9.6kWh battery could reach 74.77 % and 99.93 %. However, battery performance is constrained by PV capacity. Schram et. al [25] noted that optimal storage capacity is in the range of 0.5–9 kWh depending on PV capacity. Despite their benefits, batteries can also enhance system costs and may introduce positive environmental effects [26].

AC energy consumption accounts for a large portion of total building energy consumption. Meanwhile, occupants' thermal comfort preferences span a relatively wide temperature range. This provides an opportunity to adjust AC energy consumption to enhance the energy matching without additional investments and environmental harm [27]. Studies have explored load flexibility control strategies, such as frequency control of AC units [28], room set temperature adjustment [29], and unit start-stop control [18]. However, most existing load flexibility strategies apply uniform temperature adjustments across the entire building, failing to consider the spatial and temporal characteristics of occupants' behaviors in various types of rooms [30].

In summary, standalone optimization techniques, such as PV capacity augmentation, battery capacity expansion, and load flexibility utilization, can each enhance energy matching in PVAC systems, but their effectiveness is inherently constrained when applied in isolation. Relying on oversized PV systems fails to adapt to varying weather conditions. Solely expanding battery capacity raises investment costs and brings potential environmental risks. Uniform load flexibility control remains constrained by the existing PVAC system configuration [31,32]. Moreover, capacity design limits control flexibility, and control strategies are themselves constrained by capacity configurations. Therefore, integrating capacity optimization with control strategy optimization is essential to fully leverage the strengths of each technology and achieve real-time energy matching in PVAC systems.

1.3. Related work on the optimization methods of PVAC systems

A reasonable evaluation and optimization method is crucial for the comprehensive optimization of PVAC system capacity design and control strategy. Considerable research efforts have been devoted to developing a multi-objective optimization method for PVAC coupling systems from the perspective of energy performance. The main evaluation indicators are self-sufficiency (SS), self-consumption (SC) [33,34], solar fraction (SF) [35], zero energy potential, and coefficient of performance (COP) [36]. Li et al. achieved a 90 % energy matching degree for PVAC systems coupled with load flexibility and phase change materials (PCM) [20]. Zou et al. investigated the energy performance of PVAC systems coupled with load flexibility and batteries through SS, SC, and ZEP indicators [37]. While the energy performance of PVAC systems can be improved by unlimited expansion of PV and battery capacities, the related cost surges substantially.

Energy performance and economic efficiency are important determinants for evaluating the feasibility of the PVAC system optimization schemes [38,39]. The main evaluation indicators are total cost [40], the levelized cost of energy (LCOE) [41], and the payback period (PB) [42]. Aguilar et al. demonstrated that application of PVAC systems can lead to a 16 % reduction in the annual average cost [43]. Leite et al. conducted an economic feasibility analysis of PVAC systems in different regions and found that the maximum internal rate of return can reach 29 % [44]. Considering that the building industry accounts for a large part of carbon emissions, the environmental performance of PVAC systems, particularly carbon emission reduction, has received increasing attention [45]. Aguilar et al. demonstrated that the use of PVAC system can mitigate carbon emissions by 112.94 kg throughout the cooling season [46]. Wang et al. showed that the CO_2 emission reduction coefficient of PVAC systems could reach up to 919.34 g CO_2-eq./kWh, and this coefficient was directly proportional to the PV capacity. However, existing studies often consider energy, economic, or environmental objectives in isolation in PVAC system optimization, and fail to resolve their inherent conflicts [47].

In summary, there are many methods for evaluating and optimizing the capacity design and control strategy of PVAC systems, such as improving energy performance, enhancing economic efficiency, and reducing carbon emissions [48,49]. Whereas, in practice, the operational conditions of PVAC systems are highly complex and continuously fluctuating. This renders the evaluation and optimization methods that are based solely on a single perspective, even when incorporating multiple indicators, ineffective in facilitating the comprehensive enhancement of the overall system performance [50]. Therefore, it is necessary to develop an evaluation and optimization method for the capacity design and energy control strategy of PVAC coupling systems that takes into account energy, economy, and environment, in order to improve the overall performance of the system.

1.4. Gap and proposed solution

As shown in Table 1, based on the above literature review, existing research has already involved the capacity and energy control strategy optimization of PVAC systems. However, some problems of the system optimization are still not addressed. Firstly, few studies on load flexibility control strategies consider the spatiotemporal characteristics of occupant behavior across different rooms. Secondly, despite the complex interconnections between PV, battery, and AC capacity design and control strategies, integrated optimization of these elements in PVAC systems is rarely explored. Thirdly, evaluation and optimization methods for such systems often focus solely on energy performance, with little consideration of economic and environmental aspects. Finally, a hierarchical multi-objective co-optimization of capacity design and control strategy for PVAC systems coupling with batteries and load flexibility has not yet been proposed.

To address these gaps, this study proposes a hierarchical multi-objective co-optimization framework for PVAC systems. This framework simultaneously integrates capacity design and control strategy optimization while balancing energy, economic, and environmental objectives. This work makes three significant contributions to PVAC

Table 1
Comparison of research status with the content of this article.

Study	Method	Indicator	Limitations
Li et al [9]; Zhao et al [51]; Huang et al [52]; Loem et al [53]; Chen et al. [54]	PV/battery capacity optimization	Energy (SS, SC, RZEP, COP)	Ignored occupant behavior; overlooked economic and environmental performance
Opoku et al [23]; Mahmoudi et al [41]; Aguilar et al [43]; Leite et al [44] ; Zhao et al. [51]	PV capacity optimization	Energy (PV utilization) Economic (NPV, PB)	Neglected environmental performance; no capacity-control integration
Wang et al [45]; Aguilar et al [55]; Su et al [56]; Wang et al. [57]	PV capacity optimization	Environmental	Single objective; ignored interactions between capacity and control
This work	Co-optimization of PV/battery capacity + control strategy (incorporating occupant behavior)	Energy ($TCSR, GP_{total}$) Economic (NPV, PB) Environmental (ER)	Multi-objective optimal solution is obtained by comprehensively weighing the conflicts of different performances

system optimization. A three-stage control strategy of load flexibility, battery, and grid were developed with spatiotemporal occupancy characteristics. A"3E" evaluation method is established, using unified metrics (TCSR, GP_{total}, NPV, ER) to holistically assess system performance. A hierarchical multi-objective co-optimization method for PVAC systems was proposed to resolves capacity design and control strategy interdependencies.

In this paper, section 2 presents a system description and modelling of PVAC coupling systems. Section 3 presents the co-optimization framework of the PVAC systems coupled with load flexibility, batteries, and the utility grid, including the physical models, different control strategies, 3E evaluation methods, and multi-objective optimization methodology. Section 4 discusses the results of the optimization methods. Section 5 presents the key conclusions.

2. System description and modelling

2.1. System description

In this study, the PVAC coupling system primarily consists of PV array, battery, air conditioning (AC) units and building (load), as shown in Fig. 1. In the building, there are three types of functional rooms consisting of offices, meetings, and classes in the building. Occupant mobility exhibits distinct spatial-temporal patterns in different rooms and different periods. Moreover, occupants' thermal comfort temperature ranges from 22.6 °C to 29.4 °C. The building load can be adjusted to change the power consumed by AC units. The power flow is described as follows: PV power directly drives AC units, as well as supplies to the battery and is fed into the utility grid. The battery can store energy from both AC units, PV array and utility grid and discharge power to AC units. The utility grid can supply power to AC units and batteries.

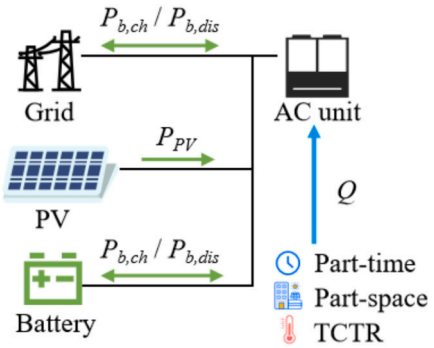

Fig. 1. Schematic of the PVAC coupling system in building.

2.2. Modelling

2.2.1. Building model

The PVAC systems were implemented in a U-shaped office building located in Hunan Province, oriented along an east-west axis (17.85° east by north). The total area of the building is 2399 m^2, which is shown in Fig. 2. The heat transfer coefficients of the building envelope are shown in Table 2. The building features various types of rooms, including offices, meeting rooms, and classrooms. Regarding the offices, the areas facing east, south, west, and north are 0 m^2, 503.58 m^2, 337.68 m^2, and 450.78 m^2, respectively. For the meeting rooms, the corresponding areas for the east, south, west, and north orientations are 0 m^2, 168 m^2, 0 m^2, and 319.44 m^2, respectively. Additionally, for classrooms, the areas in the east, south, west, and north directions are 0 m^2, 619.5 m^2, 0 m^2, and 0 m^2, respectively.

2.2.2. PVAC model

In this study, a grid-connected PVAC system was implemented in the building to investigate energy, economic, and environmental performance. The PV system is installed on the roof with a fixed tilt angle according to the location, directly. The personnel, lighting, and equipment parameters in different rooms were selected according to the public building energy efficiency standards. The PVAC system means that the power generated by the PV system is used by the air conditioning directly. The indoor temperature conditioned by the PVAC system is mainly determined by the real-time PV generation. The thermal comfort temperature range can be from 22.6 °C to 29.4 °C. When the indoor temperature conditioned by the PVACs is within the thermal comfort temperature range (TCTR), this moment is regarded as the real-time energy matching time. When the indoor temperature is beyond the temperature range, the insufficient or surplus electricity can be provided by the batteries and utility grid.

To enhance AC load flexibility, a part-time part-space (PTPS) operation model of PVAC systems was developed, integrating the spatial and temporal characteristics of occupants' behaviors in various types of rooms and thermal comfort temperature ranges. In the building, there are various types of functional rooms consisting of offices (office, studio, and attended archive room), meetings (conference room and lecture hall), and classes (classroom and computer room). Under the PTPS operation model, the AC operation schedules and temperature setpoints can be adjusted across these zones. The temporal and spatial occupancy characteristics in different rooms were obtained through actual occupancy patterns. For offices and classrooms, the operation schedules were derived from working hours and academic timetables, respectively. For meeting rooms, the operation schedules were determined by the actual booking records, which exhibited irregular usage patterns due to intermittent reservation demands.

2.2.3. Battery model

In this study, a simplified battery charging and discharging model was used to improve the energy matching of PVAC systems. Charging is constrained by a maximum state of charge (SOC) of 80 % of capacity, while discharging is limited to a minimum SOC of 20 % of capacity. The parameters of the battery are shown in Table 3.

The service life of batteries is closely related to charge - discharge

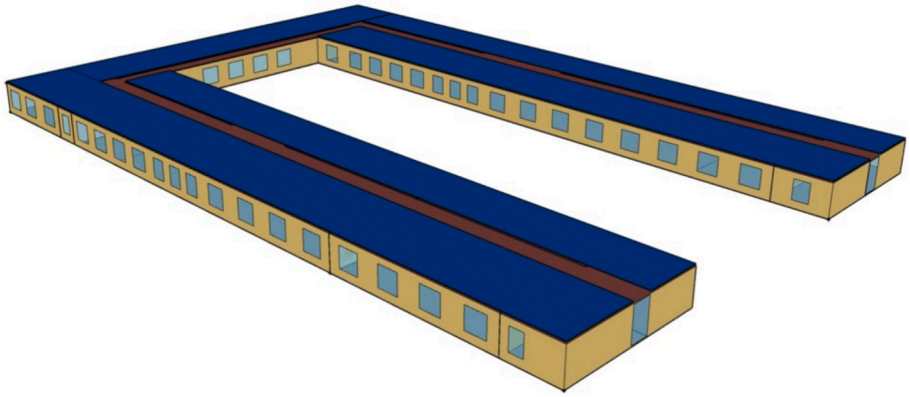

Fig. 2. The layout of the office building.

Table 2
The heat transfer coefficients (K) of the envelope structures in the building.

Construction	Unit	Value
Roof	W/(m^2•K)	0.64
Exterior wall	W/(m^2•K)	1.00
Exterior window	W/(m^2•K)	2.80
Interior wall	W/(m^2•K)	1.64
Floor	W/(m^2•K)	0.80

Table 3
The electrical parameters of the battery model.

Parameter	Unit	Value
Capacity	kWh	5
Rated charging power	kW	3.58
Rated voltage	V	51.2
Rated current	A	20
Transient peak current	A	200
Number of batteries		32
Charging efficiency	–	≥95 %

depth and cycle number. The state of charge (SOC) is used to indicate and limit battery operations. The calculation formulas for the batter charging and discharging state are shown in Eq. (1) to Eq. (4) [58].

$$SOC_{(t+1)} = SOC(t) + \varsigma \frac{P_{b,ch}(t)\Delta t \eta_{ch}}{E_b(t)} - (1-\varsigma)\frac{P_{b,dis}(t)\Delta t}{Eb(t)\eta_{dis}} \quad (1)$$

$$SOC_{\min} \le SOC(t) \le SOC_{\max} \quad (2)$$

$$0 \le P_{b,ch} \le P_{ch,\max} \quad (3)$$

$$0 \le P_{b,dis} \le P_{dis,\max} \quad (4)$$

Where $P_{b,ch}$ is the battery charging power (kW), $P_{b,dis}$ is the discharging power (kW), η_{ch} is the charging efficiency, η_{dis} is the discharging efficiency, $\varsigma$is the charging stage, $Eb(t)$ is the stored power (kWh), Δt is the timestep.

2.2.4. Model verification

In this study, the real-time energy generation and consumption of PVAC system simulation have been verified. An experimental platform for PVAC systems was built in Hunan province (28.19°N , 112.98°E), as shown in Fig. 3. The experimental platform consists of two rooms, equipped with PV systems, air conditioning systems, batteries, data acquisition systems, central energy control systems, and terminal monitoring systems. Technical specifications of the PVAC systems are systematically documented in Tables 4 and 5, respectively. The laboratory spatially configured two spaces: Room 1 (8.7 m north-south × 3.8 m east-west × 3.5 m height) and Room 2 (7.0 m north-south × 5.0 m east-west × 3.5 m height).

Fig. 4 illustrates the dynamic power variation and indoor temperature comparison of PVAC systems with PTPS model and the traditional operation model. The traditional model enforced uniform 26 °C setpoints across all rooms and periods. On July 6th and 7th, energy control strategies under both models were evaluated, revealing distinct discrepancies in PV generation-AC consumption alignment. The traditional model exhibited pronounced energy mismatching between PV generation and AC energy consumption, resulting in SS and SC values of 78.54 % and 82.24 %, respectively. In contrast, the PTPS model adjusted AC consumption to achieve a significantly stronger correlation with PV generation, elevating SS and SC to 88.87 % and 90.29 %. The load flexibility control strategy with PTPS model yields further improvement in the real-time energy matching of PVAC systems.

3. Methodology

3.1. Research framework

The hierarchical multi-objective co-optimization framework for PVAC systems addresses the combined impacts of load flexibility, battery capacity, PV capacity, and grid interaction strategies, all of which influence real-time energy matching performance, economic viability, and carbon mitigation potential. As show in Fig. 5, this framework comprises two optimization layers sharing unified evaluation metrics and operates through an iterative feedback mechanism, including thermal comfort satisfaction ratio (TCSR), and grid cumulative action power (GPtotal), net present value (NPV), and emission reduction (ER). Through parametric and iterative processes, the optimized PV and battery capacity with an optimized three-stage control strategy considering spatial-temporal occupancy features are obtained.

(a) Upper layer-Control strategy optimization

This layer develops coordinated energy management through three stages, which includes strategies of load flexibility regulation, battery storage dispatch, and the utility grid interaction.

Stage 1: The strategy of load flexibility is optimized by considering spatial-temporal occupancy features that incorporates real-time load demand profiles in different rooms, thermal inertial of buildings, and occupancy comfort constraints.

Stage 2: Battery dispatch integrated with optimized load flexibility to enhance real-time energy matching.

Stage 3: Grid interaction (off-grid/grid-connected modes) is activated to leverage surplus PV export or grid power import, thereby avoiding over-reliance on oversized batteries.

Fig. 3. PVAC experimental platform with PTPS operation model.

Table 4
PV system parameters.

parameters	unit	value
cell type	–	polysilicon
maximum power	W	550
short-circuit current	A	13.97
open-circuit voltage	V	49.82
Panel numbers	–	22

Table 5
AC system parameters.

parameters	unit	value
model	–	MDM0610-E2
rated cooling capacity	kW	20
max cooling power	kW	9.6
rated cooling COP	–	5.88

(b) Lower layer- Capacity optimization

This layer is dedicated to capacity optimization for PV systems and batteries within predefined parameter ranges, using multi-objective functions targeting energy performance, economic viability, and environmental impact.

The two layers achieve iterative co-optimization through parametric refinement. The lower layer transmits optimized PV and battery capacity to the upper layer, which then feeds back corresponding performance metrics. Through successive optimization cycles, the framework gradually converges on solutions that simultaneously optimize both capacity design and control strategy.

In the multi-objective hierarchical co-optimization for PVAC systems, the workflow can be divided into 5 steps:

In step 1, the physical model of the building and PVAC systems was established by EnergyPlus software. The PV generation is mainly determined by the real-time radiation intensity and power generation efficiency of the PV array. The AC unit was modeled as an ideal air conditioning system with a nominal coefficient of performance (COP) of 3.5, directly powered by real-time PV generation. The battery charging and discharging model was established by Python. These models and parameters provide a foundational basis for subsequent control strategy

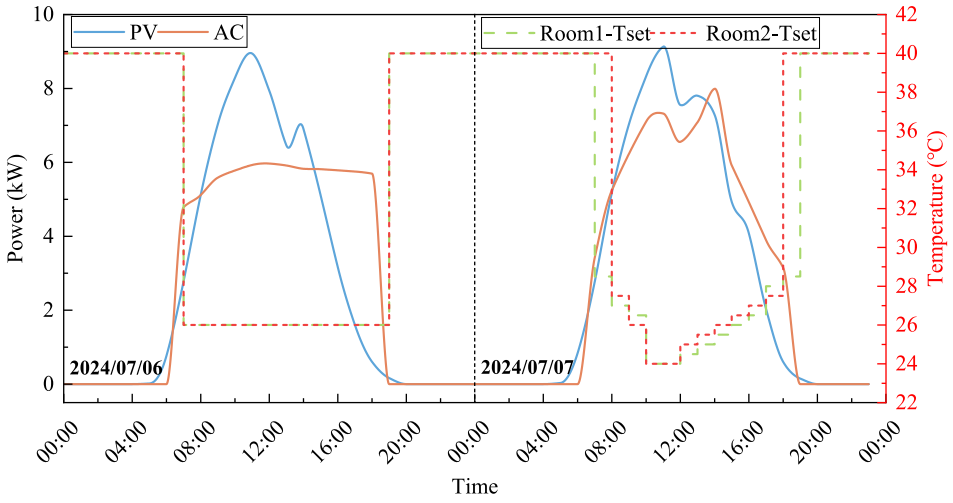

Fig. 4. Power variation and indoor temperature conditioned by PVACs with different operation models.

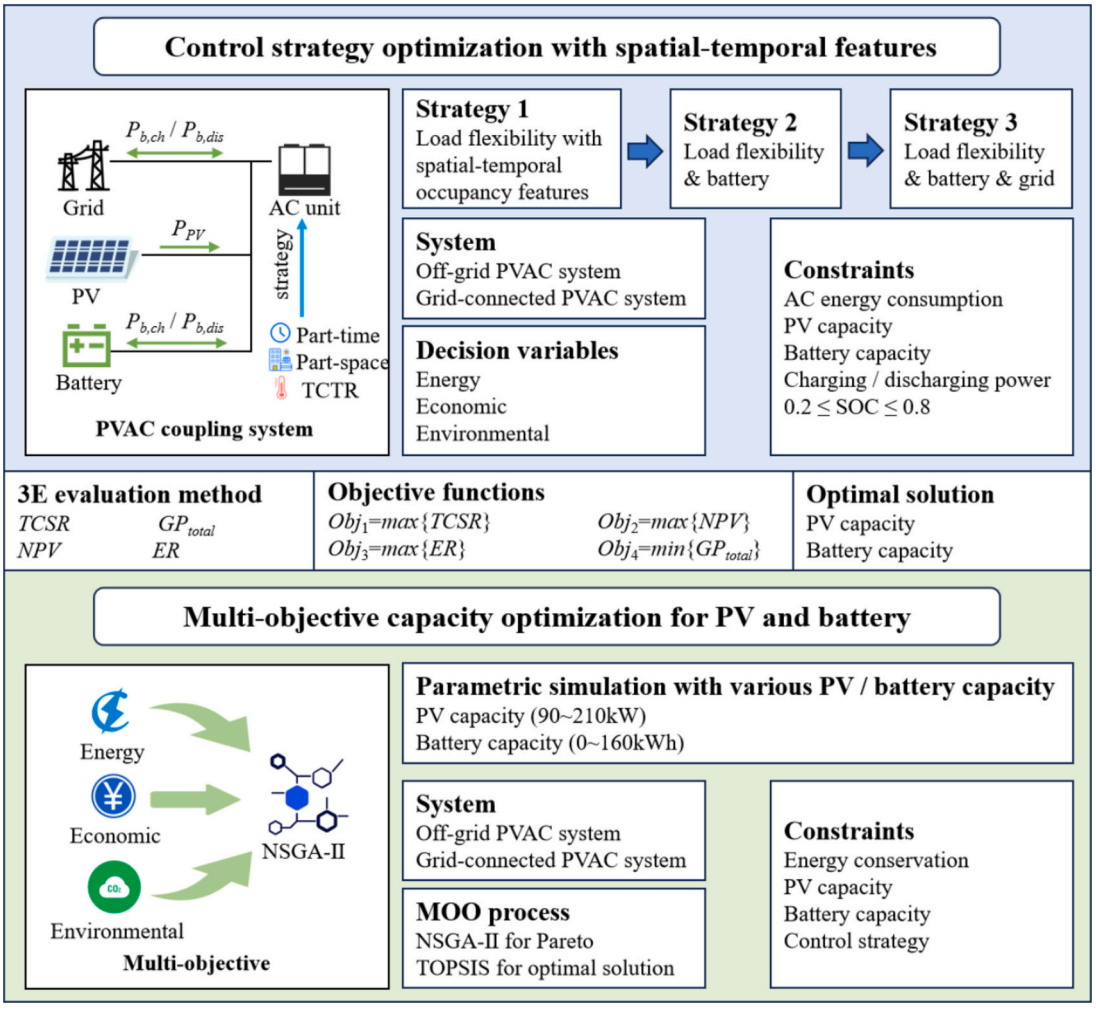

Fig. 5. The optimization framework of PVAC system with load flexibility, batteries, and utility grid.

formulation and performance simulation.

In step 2, three energy control strategies were formulated. Based on the spatial-temporal occupancy characteristics and thermal comfort constraints, a three-stage control strategy is developed, including load flexibility regulation, battery dispatch, and grid interaction.

In step 3, a 3E evaluation method for PVAC coupling systems was developed from energy, economic, and environmental perspectives, covering energy performance indicators (TCSR, GP_{total}), economic indicators (NPV, payback period), and environmental indicators (ER), which serve as the objective function for the optimization process.

In step 4, a parametric study of PVAC systems with different capacities of PV and battery was conducted under different energy control strategies. The parametric simulation process was based on EnergyPlus and the Extreme Gradient Boosting (XGBoost) algorithm with Python. The PV capacity ranges from 90 to 210 kW with increments of 15 kW, the battery capacity ranges from 0 to 160 kWh with increments of 10 kWh.

In step 5, a multi-objectives co-optimization method was presented for the PVAC systems. Two objective variables and four objective functions were carefully selected for the multi-objective optimization analysis by NSGA - II. Subsequently, the TOPSIS algorithm was employed to provide a single optimal solution for practical decision-making.

3.2. Optimized control strategies

The proposed energy control strategies prioritize real-time energy matching in PVAC systems to minimize PV curtailment and gird disturbance through a hierarchical three-stage approach. The load flexibility was first adopted according to the temporal and spatial occupancy characteristics and thermal comfort temperature range. Then, the batteries were implemented to increase the real-time energy matching degree. Lastly, the interaction with the utility grid was considered to avoid the high cost of the system by oversized batteries.

3.2.1. Control strategy of load flexibility

The load flexibility strategy is optimized by considering spatial-temporal occupancy features that incorporate real-time load demand profiles in different rooms, thermal inertia of buildings, and occupancy comfort constraints. The total output capacities of AC units are dynamically matched to real-time PV generation. Then, the initial cooling energy distribution is determined by the temporal and spatial characteristics of the occupants' behavior and areas of different rooms. If the indoor temperature conditioned by PVAC systems deviates from the predefined thermal comfort temperature range, an energy redistribution is activated. In the redistribution strategy, the energy is shifted from the room with the lowest temperature to the room with the highest temperature. Energy is allocated in increments of 30 Wh at each interval, and the indoor temperature in each room is subsequently recalculated. The process continues until thermal comfort compliance is maximized. The utilization of load flexibility can effectively enhance the real-time energy matching without capital expenditure. Nevertheless, constrained by the rated output capacity of the AC and thermal storage capacity of the envelopes, it is challenging to achieve 100 % real-time energy matching degree of the PVAC system.

3.2.2. Two-stage control strategy of load flexibility and battery

Battery integration can further increase the real-time energy matching combined with the load flexibility control strategy. The control strategy of PVAC systems with load flexibility and battery was illustrated in Fig. 6. Firstly, the strategy initiates by identifying rooms requiring cooling based on the dynamic behavior of occupants. The indoor temperatures of each room were predicted by the load flexibility control strategy and XGBoost algorithm. Then, if there are rooms whose temperatures exceed the thermal comfort range and the battery has the capacity space for charging or discharging, the energy control strategy of batteries is activated. For overheating rooms, the battery discharges to increase the power output of AC units to decrease indoor temperatures. For overcooling rooms, the power output of AC units was curtailed with the surplus energy charging batteries. However, achieving 100 % real-time energy matching requires a large capacity battery, resulting in poor economic performance. To optimize the overall performance, it is highly advisable to consider interaction with the utility grid.

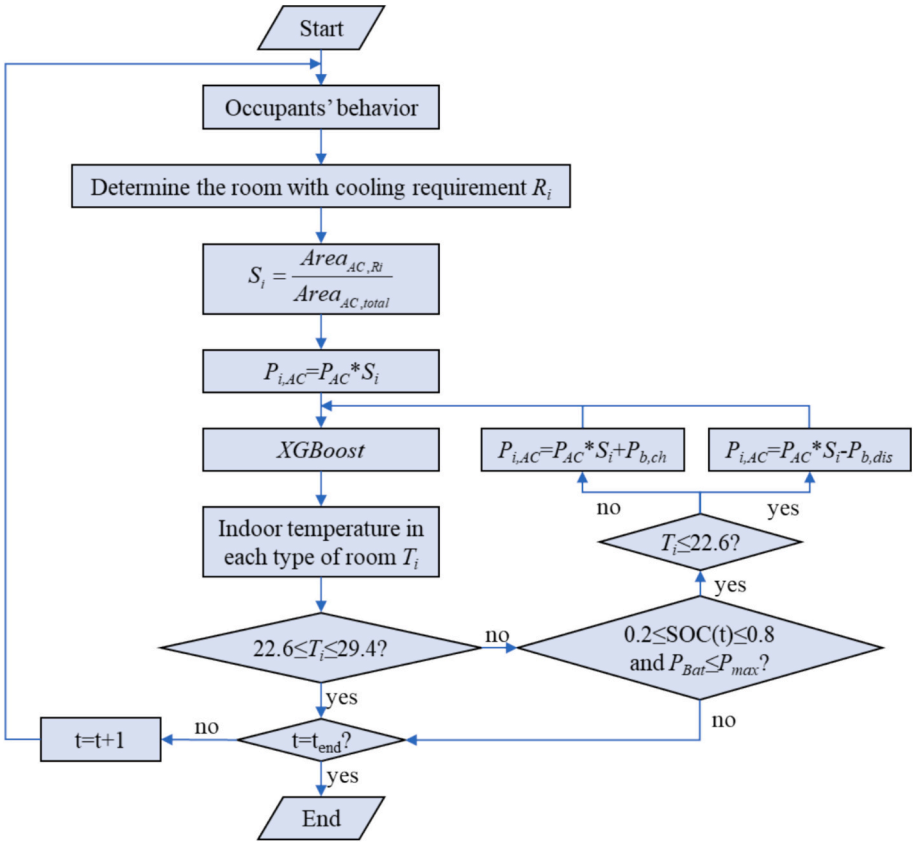

Fig. 6. Energy control strategy with load flexibility and battery.

3.2.3. Three-stage control strategy of load flexibility, battery, and grid

Based on the optimized control strategy of load flexibility and battery, the grid interaction strategy adopted in this study is self-consumption with surpluses, in which part of the PV generation is prioritized for on-site use, with excess energy exported to the grid. The energy control strategy of PVAC systems with load flexibility, battery, and utility grid was shown in Fig. 7. Under scenarios where batteries cannot balance system energy generation and consumption, the energy control strategy of the utility grid is activated. For overheating rooms, the system can draw a certain amount of electricity from the utility grid to increase the power output of the AC units. For overcooling rooms, the system can reduce the power output of the AC units, and the surplus PV generation can be fed into the grid.

3.3. 3E evaluation method

In this study, the capacity optimization of PV and batteries under an optimal three-stage control strategy of PVAC coupling system mainly aims to simultaneously increase the energy, economic, and environmental performance of the PVAC coupling system. During the capacity optimization process, a comprehensive evaluation method was developed to assess the PVAC coupling system across energy (e.g., thermal comfort satisfaction ratio (TCSR) and grid cumulative action power (GP_{total})), economic (e.g., net present value (NPV) and payback period (PB)), and environmental aspects (emissions reduction (ER)).

3.3.1. Energy performance evaluation

In the PVAC system, the real-time PV generation was directly used to drive the air conditioning. Considering the load flexibility, if the indoor temperature conditioned by the PVAC system satisfies the indoor comfort requirements, the moment can be regarded as the real-time energy matching hour. In this study, the energy performance evaluation indicator is the thermal comfort satisfaction ratio, which represents the ratio of real-time energy matching time to the total operating time of the AC. The calculation formula is presented in Eq. (5). The TCSR value varies within the range of 0 to 1. If the TCSR is lower than 1, it means that during the AC operation period, the PVAC system cannot completely satisfy the thermal comfort requirements of each room in the building.

$$TCSR = \frac{\sum t_{comfort}}{\sum t_{AC}} \tag{5}$$

Where, $t_{comfort}$ represents the number of hours that the indoor temperature is in the thermal comfort temperature range, h.

In the grid-connected PVAC system, the indoor temperature conditioned by the PVAC system can fully satisfy the indoor comfort requirements. However, the energy fluctuations of the PVAC systems can impose a significant impact on the utility grid, involving the injection of excess PV generation into the grid and the power extraction of AC from the grid. In this study, the grid cumulative action power (GP_{total}) was used to evaluate the energy performance of the grid-connected PVAC system. The calculation formula is presented in Eq. (6).

$$GP_{total} = \sum_{i=1}^{n} |P_i| \tag{6}$$

Where, P_i represents power uploaded to the grid or the power extraction from the grid, W; i represents the operation hour.

3.3.2. Economic performance evaluation

The economy of the PVAC system is crucial for its development. In this study, the economic evaluation indicators are net present value (NPV) and payback period (PB). NPV is calculated as the sum of the

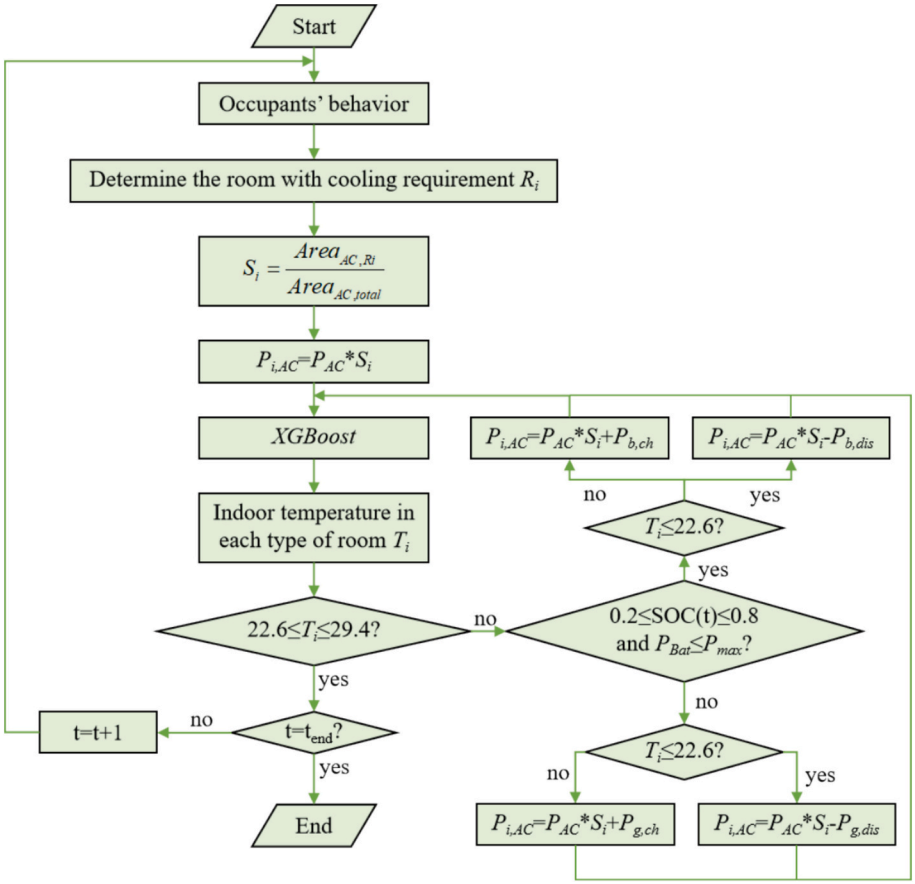

Fig. 7. Control strategy of load flexibility, battery, and utility grid.

present values of all future cash inflows and outflows associated with an investment or project over its entire lifespan, as shown in Eq. (7) [59]. The PB consists of the static payback period (SPB) and dynamic payback period (DPB). SPB is the time needed to recover the initial investment through net earnings, without accounting for the time value of money, as shown in Eq. (8) [59]. The DPB considers the time value of money, as shown in Eq. (9) [59].

$$NPV = \sum_{n=0}^{N}(F_{CI} - F_{CO})_n(1+k)^{-n} \tag{7}$$

$$\sum_{n=0}^{N_S}(F_{CI} - F_{CO})_n = 0 \tag{8}$$

$$\sum_{n=0}^{N_D}(F_{CI} - F_{CO})_n(1+k)^{-n} = 0 \tag{9}$$

Where N represents the operating years of the system; F_{CI} represents the cash inflow; F_{CO} represents the cash outflow; $(F_{CI}$ -$F_{CI})_n$ represents the cash flow in the n year; k is the discount rate.

3.3.3. Environmental performance evaluation

The adoption of the PVAC system can effectively reduce greenhouse gas emissions by decreasing the energy consumption of buildings. The environmental evaluation indicator is to minimize greenhouse gas emissions, especially CO_2 emissions. The total CO_2 emissions reduction (ER) is selected as the environmental indicator in this study, which is shown in Eq. (10).

$$ER = (m_{CD} + m_{CO_2} + m_{SO_2} + m_{NO_x}) \times E_{PV} \tag{10}$$

Where m_{CD}、m_{CO_2}、m_{SO_2}、m_{NO_x}represent the masses of carbon dust, carbon dioxide, carbon dioxide, and nitrogen oxides produced by each kilowatt-hour of electricity generated by traditional thermal power plants.

3.4. Multi-objective capacity optimization of PV and battery

In this study, a multi-objective capacity optimization of PV systems and batteries is established considering energy, economic, and environmental benefits. The formulation of the optimization process composed of decision variables, objective functions as well as constraints has been implemented. As shown in Fig. 8, the optimization process is principally composed of five sequential steps: pre-data input, system performance analysis, multi-objective optimization process, optimal solution decision-making process, and optimal solution output.

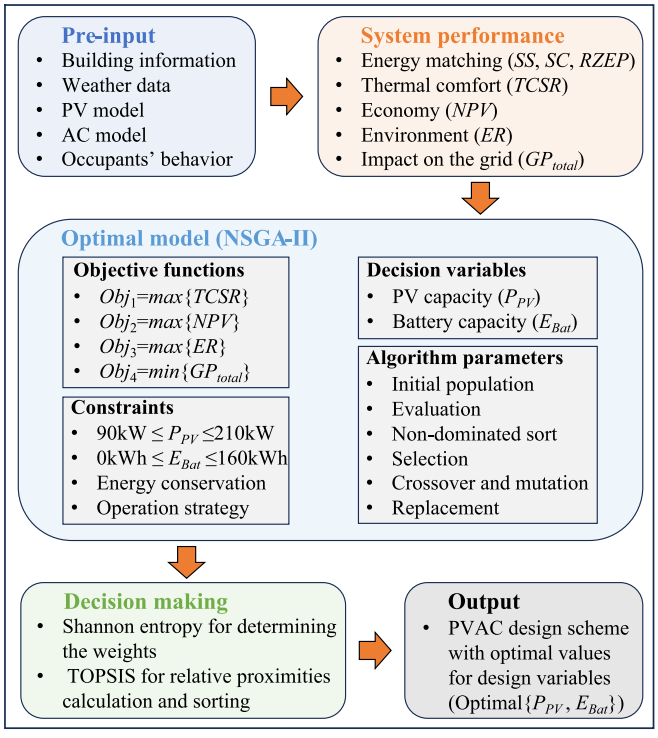

Fig. 8. Multi-objective optimization of the PVAC coupling system.

In the pre-data input stage, EnergyPlus serves as the core simulation tool, integrating diverse parameters including building attributes, weather data, PV and AC system models, and dynamic occupancy patterns across different rooms. This integration enables the software to simulate and output real-time data on PV power generation and AC energy consumption.

In the system performance stage, the energy, economic, and environmental performance of the PVAC systems was calculated with optimal energy control strategies and different capacities of PV systems and batteries. These performance datasets serve as critical inputs for subsequent multi-objective optimization algorithms.

In the multi-objective optimization stage, the comprehensive optimization model of PVAC coupling systems is established with four objective functions, two decision variables (PV capacity and battery capacity), and four constraint conditions. Subsequently, the relevant parameters of the NSGA-II algorithm are configured, which are shown in Table 6. Through the computation of the NSGA-II algorithm, a set of Pareto fronts, namely a series of alternative optimal solutions, can be derived.

In the optimal solution decision-making stage, the Shannon entropy method is employed to quantify the weights among different objective functions. Subsequently, the TOPSIS algorithm is utilized to allocate the corresponding weight values and compute the distance from each solution within the Pareto front to the ideal solution. Finally, all solutions are ranked based on their proximity to the ideal solution, and the optimal solution is thereby output.

In the final step, under the optimal three-stage control strategy, the optimal capacities of PV and batteries for the PVAC coupling system were successfully derived.

4. Results and discussion

4.1. Energy performance comparison for different PVAC systems

4.1.1. Energy performance of off-grid PVAC coupling system

Adopting load flexibility based on dynamic occupants' behavior and thermal comfort temperature range across different rooms and batteries significantly impacts the real-time energy performance of the PVAC systems. Besides the optimal energy control strategy of load flexibility and batteries, the varying capacities of PV systems and batteries also critically influence the indoor temperature conditioned by the PVAC coupling system. The details about the energy performance of the PVAC coupling systems with different capacities of PV systems and batteries are described as follows.

Fig. 9 shows the thermal comfort satisfaction ratio (TCSR) of the PVAC coupling systems with different capacities of PV systems and

Table 6
Basic Parameter Settings of NSGA-II.

Parameter	Value
Number of Decision Variables	2
Number of Objective Functions	4
Population Size	1000
Number of Generations	200
Selection Method	Tournament Selection
Number of Elite Individuals Preserved for the Next Generation	30
Crossover Probability	0.9
Mutation Probability	0.1

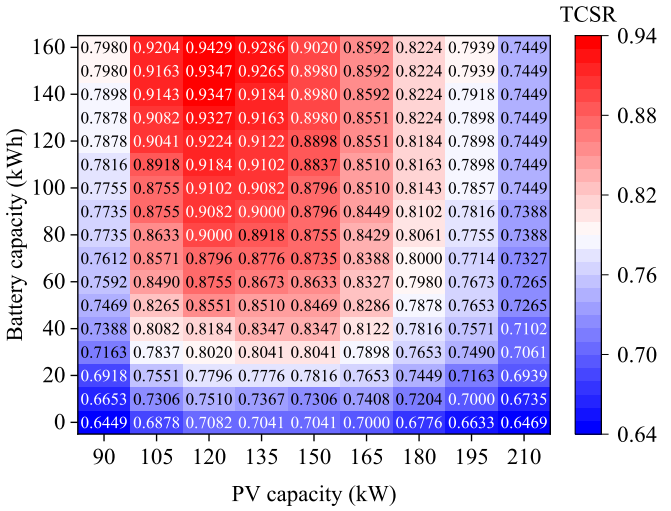

Fig. 9. The energy performance of PVAC coupling system with different capacities.

batteries. When the PVAC systems are only equipped with load flexibility and varying PV capacities, TCSR initially rises with increasing PV capacity. The maximum TCSR value occurs when the PV capacity reaches 120 kW. With the optimal PV capacity, the ratio of total PV generation to total AC energy consumption is only 0.8, demonstrating the load flexibility control strategy can effectively enhance the real-time energy performance of PVAC systems based on the dynamic behavior of occupants and thermal comfort requirements. When PV capacity is beyond 120 kW, excessive PV generation induces overcooling problems and causes a lower TCSR value.

As illustrated in Fig. 9, batteries can effectively increase the TCSR value. Under the premise that the PV capacity is 90 kW, the TCSR value can be improved by 2.04 % with a 10 kWh battery. When the battery capacity reaches 120 kWh, the TCSR value attains its peak of 79.80 %. Notably, although the TCSR gradually increases with the growth of batter capacity, its growth rate gradually decreases. When the battery capacity increases from 0 kWh to 20 kWh, the TCSR increases by 5.04 %. In contrast, when it increases from 140 kWh to 160 kWh, the TCSR only increases by 0.67 %. Under a fixed PV capacity, initial battery deployment effectively adjusts real-time energy distribution to improve TCSR. However, oversized batteries encounter some issues. For instance, there may be insufficient PV generation to charge the battery. Moreover, with the implementation of the load flexibility control strategy, the AC energy demand requirements for meeting the indoor thermal could be reduced to some extent, causing smaller capacity requirements of batteries.

Upon conducting a comprehensive analysis of PV capacity and battery capacity, the TCSR value is affected in complex ways. At the optimal PV capacity of 120 kW, TCSR rises from 0.6878 to 0.7551 with 20 kWh battery deployment. However, when the battery capacity increases from 140 kWh to 160 kWh, the increment of TCSR is only 0.0082. At 90 kW PV capacity, the increment of TCSR is smaller with the same increment of battery capacity. In addition, PV capacity shows different impacts on TCSR under different battery capacities. When the battery capacity is small, the increase in PV capacity has a relatively minor impact on TCSR. Conversely, when the battery capacity is large, the increase in PV capacity exerts a more significant influence on TCSR. This nonlinear behavior underscores the necessity for co-optimizing PV and battery capacities. The optimal configuration consists of a 120 kW PV capacity and a 160 kWh battery capacity, enabling the TCSR to reach 94.29 %.

As shown in Fig. 9, it is evident that multiple combinations of PV capacity and battery capacity for the PVAC coupling system can achieve the same TCSR value. To clearly illustrate the relationship between PV and battery capacities under the same TCSR value, a contour plot has been created in Fig. 10. The horizontal axis represents the variation in PV capacity, and the vertical axis represents the change in battery capacity. The TCSR values are denoted by contour lines and color gradients, where warmer colors represent higher TCSR values and cooler colors represent lower ones. In terms of the overall change trends of PV capacity and battery capacity on TCSR value, an upward trend in PV capacity directly increases TCSR as augmented PV generation can meet more AC energy consumption. Meanwhile, an increment in battery capacity also results in a rise in the TCSR, owing to the fact that batteries with larger capacities exhibit enhanced capabilities in regulating the energy matching degree of the PVAC system.

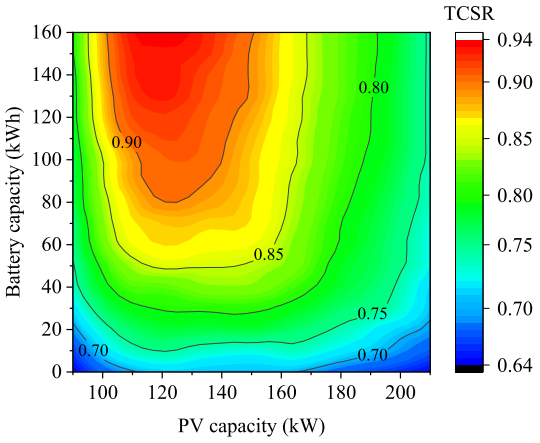

Fig. 10. The contour map of PVAC coupling system with different capacities.

4.1.2. Energy performance of grid-connected PVAC coupling system

From the above discussion of the off-grid PVAC system coupled with load flexibility and batteries, it is difficult to fully satisfy the real-time indoor thermal comfort only by the PVAC coupling system. It still needs to rely on the power grid to supplement the insufficient power or absorb the excess power. The energy performance of the grid-connected PVAC coupling systems was evaluated by the grid cumulative action power (GP_{total}) under different capacities of PV systems and batteries.

As shown in Fig. 11 and Fig. 12, an upward trend in PV capacity directly increases the GP_{total} value. Given the inherent instability of PV generation, a PV system with a relatively high capacity may exert a greater impact on the utility grid. However, once the battery capacity surpasses 20 kWh, the GP_{total} value initially decreases as the PV generation rises. The reason is that a larger-capacity battery can mitigate the fluctuations in PV generation. The grid-connected PVAC coupling

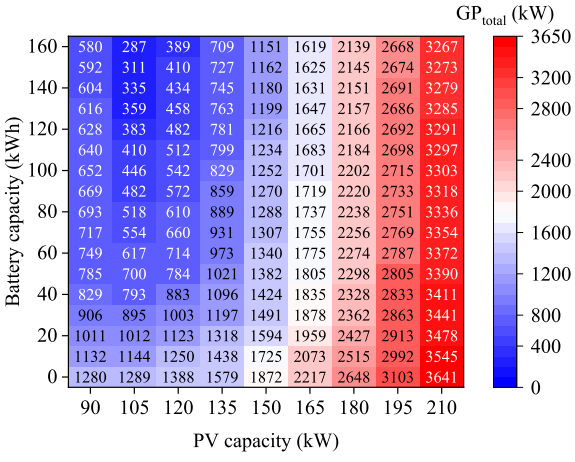

Fig. 11. The energy performance of grid-connected PVAC coupling system with different capacities.

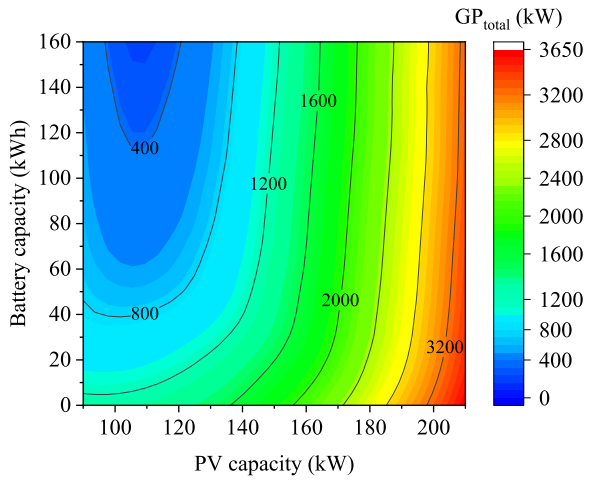

Fig. 12. The contour map of grid-connected PVAC coupling system with different capacities.

system attains a higher level of energy matching, thereby reducing the impact on the utility grid. Nonetheless, as PV capacity continues to grow, the regulating capacity of batteries becomes inadequate to effectively mitigate the fluctuations in PV generation. Consequently, the GP_{total} value of the PVAC coupling system begins to increase. When the PV capacity remains constant, an increase in battery capacity generally leads to a downward trend in the GP_{total}. The integration of batteries can result in a reduction of 1002.4 kW in the GP_{total}. This clearly demonstrates that an increase in battery capacity can effectively reduce the system's impact on the utility grid.

From Fig. 11, the minimum GP_{total} value of 286.6 kWh is obtained through the combination of 105 kW PV capacity and 160 kWh battery capacity. As shown in Fig. 12, the TCSR value is relatively high under the capacity combination of PV systems and batteries. This implies that the interaction duration of the utility grid is shorter to optimize thermal comfort. Additionally, the low PV capacity results in a relatively small amount of power being interacted with the utility grid. This result underscores the necessity of implementing the optimal energy control strategy of load flexibility and batteries, as well as optimizing the capacities of PV systems and batteries.

4.2. Economic performance comparison for different PVAC systems

4.2.1. Off-gird PVAC coupling system

Fig. 13 depicts the economic performance of PVAC coupling systems with varying capacities of PV systems and batteries. Regarding the overall trend, when the battery capacity remains constant, the net present value (NPV) shows a continuous upward trend as PV capacity increases. However, the growth rate of NPV generally exhibits a downward trend with the increment of PV capacity. With the fixed battery capacity, the increased PV generation can be used to meet AC energy consumption by the battery and load flexibility control strategies. Therefore, the NPV exhibits a substantial increase with the growth of the PV capacity. However, as the PV capacity continues to grow, the excess PV generation exceeds the battery's storage capacity and the limits of load flexibility, causing serious energy mismatching problems. Consequently, further increments in PV capacity led to a decline in the NPV growth rate. Under different battery capacities, the influence of PV capacity on the NPV is different. When the battery capacity is small, especially smaller than 20 kWh, an increase in PV capacity leads to a pronounced rise in the NPV. When the battery capacity is large, the increment of PV capacity results in a relatively small growth of NPV. When the battery capacity is excessively large while the PV capacity is small, the NPV turns negative. In the context of PVAC systems coupled with larger capacity batteries, real-time energy matching for the system can be achieved. However, the huge investment in batteries has a negative effect on NPV growth. Among the 153 capacity configuration combinations, the NPV reaches the peak of 356,600 CNY when the PV capacity is 210 kW and battery capacity is 0 kWh.

In the economic performance of PVAC coupling systems, the payback period is also a pivotal indicator. As shown in Fig. 14, with the increment of PV capacity, the static payback period (SPB) of PVAC systems coupled with batteries generally tends to shorten. When the PV capacity is zero,

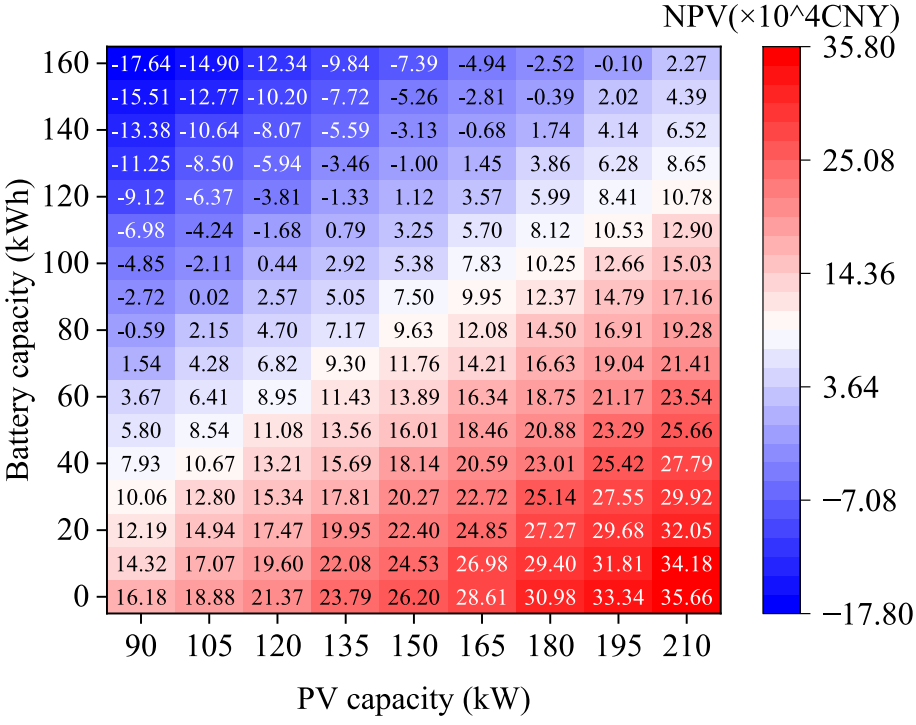

Fig. 13. The NPV of PVAC coupling system with different capacities.

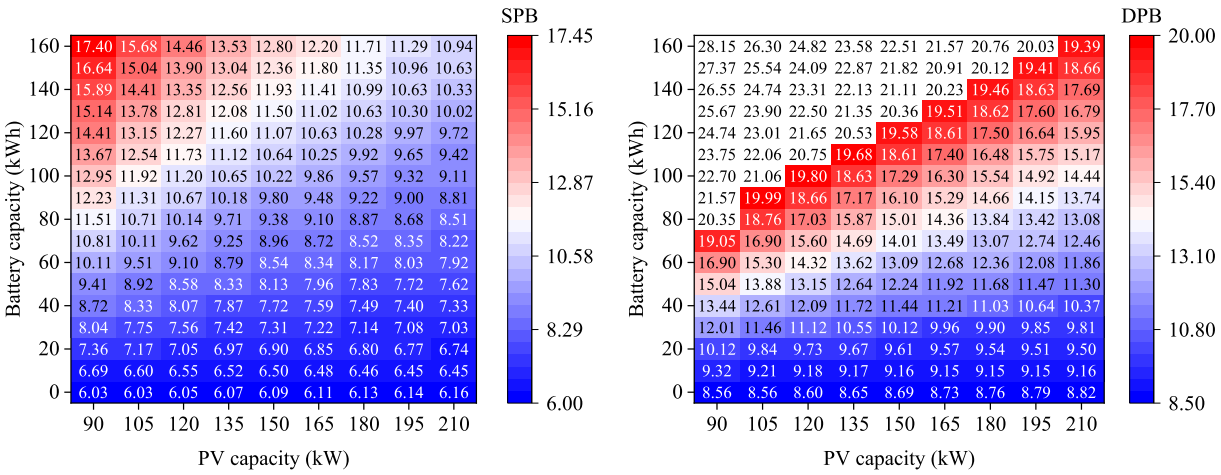

Fig. 14. The payback period of PVAC coupling system with different capacities. (a) Static payback period (b) Dynamic payback period.

the payback periods tend to lengthen as the battery capacity increases. Since the energy mismatching problem can be more serious with merely increasing PV capacity, the economic efficiency of the PVAC system decreases. Under the fixed PV capacity, the increment of battery capacity generally extends the SPB. Although large capacity batteries can alleviate energy mismatching issues, their high initial investment leads to a significant increase in the SPB value. Specifically, the shortest payback period of 6.03 years corresponds to the configuration where the PV capacity is 90 kW and the battery capacity is 0 kWh.

Compared with the SPB variation, the variation trends of the Dynamic Payback Period (DPB) are similar. Nevertheless, the DPB values are generally higher than SPB values for the same combination of PV capacity and battery capacity. This divergence is primarily attributed to the DPB's incorporation of the time value of money. Compared with SPB, DPB is more sensitive to changes in PV capacity and battery capacity. The reason is that the time value of money magnifies the impact of cost and revenue changes at different time points through DPB calculations. From the DPB, the shortest payback period is 8.56 years with the same combination of PV and battery capacity.

4.2.2. *Grid-connected PVAC coupling system*

Fig. 15 depicts the economic performance of grid-connected PVAC coupling systems. In this mode, the excess PV generation can be fed into the grid to gain a certain quantum of revenue. Regarding the overall trend, under a fixed battery capacity, the net present value (NPV) shows a continuous upward trend as PV capacity increases. When the PV capacity remains a constant value, the NPV shows a downward trend as battery capacity increases. The overall trend of grid-connected PVAC coupling systems is similar to that of off-grid PVAC coupling systems. Among the 153 capacity configuration combinations, the NPV reaches the peak of 370,500 CNY when the PV capacity is 210 kW and the battery capacity is 0 kWh. In general, since the grid-connected PVAC coupling system can sell excess PV generation for profit, the NPV value is higher than that of off-grid PVAC coupling systems under the same combination of PV capacity and the battery capacity. However, when the PV capacity is lower than 120 kW, the NPV value of the grid-connected PVAC coupling system is lower. With the low PV capacity, the import of electricity from the utility grid can enhance the grid-connected PVAC system's energy performance. Nevertheless, this practice has a negative impact on economic viability, thereby resulting in a decreased NPV. With a larger PV capacity, the excessive PV generation can be sold for profit, the NPV value is higher than that of off-grid PVAC coupling systems.

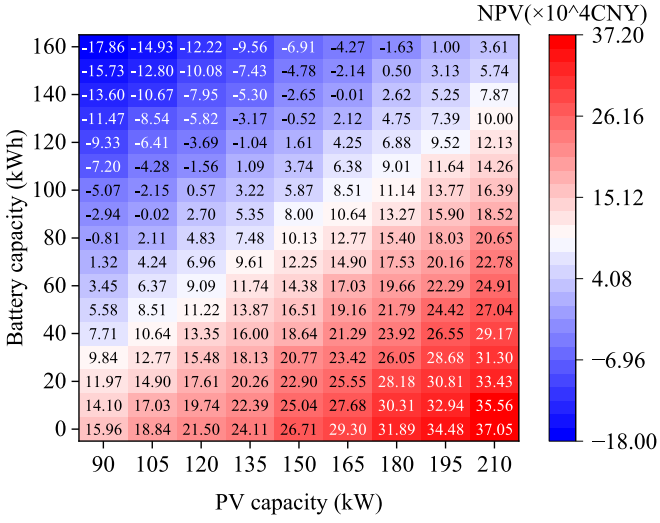

Fig. 15. The NPV of grid-connected PVAC coupling system with different capacities.

As shown in Fig. 16, the SPB and DPB variations of the grid-connected PVAC coupling system are similar to those of off-grid PVAC coupling system. The shortest payback period is 6.03 years, which corresponds to the configuration with a PV capacity of 105 kW and a battery capacity of 0 kWh. The optimal PV capacity is larger than that of off-grid PVAC coupling systems with the shortest SPB and DPB.

4.3. *Environmental performance comparison for different PVAC coupling systems*

Fig. 17 depicts the emissions reduction variations of PVAC coupling systems with different PV capacities. Overall, increasing PV capacity has a positive impact on emission reduction (ER). As PV capacity grows, it displaces more electricity generation from fossil fuels, thereby reducing ER values. In terms of environmental performance, the optimal PV capacity is 210 kW. At this capacity, the system can achieve a maximum emission reduction, including 45.79 tons of carbon dust, 167.84 tons of carbon dioxide, 5.05 tons of sulfur dioxide, and 2.53 tons of nitrogen oxides. The application of PVAC coupling systems offers a viable and efficient solution to mitigate environmental problems.

4.4. *Multi-objectives capacity optimization for different PVAC coupling systems*

From above performance analysis, there are significant conflicts among TSTR, GP_{total}, NPV, and emissions reduction (ER). Thus, this study conducts a hierarchical multi-objective co-optimization for

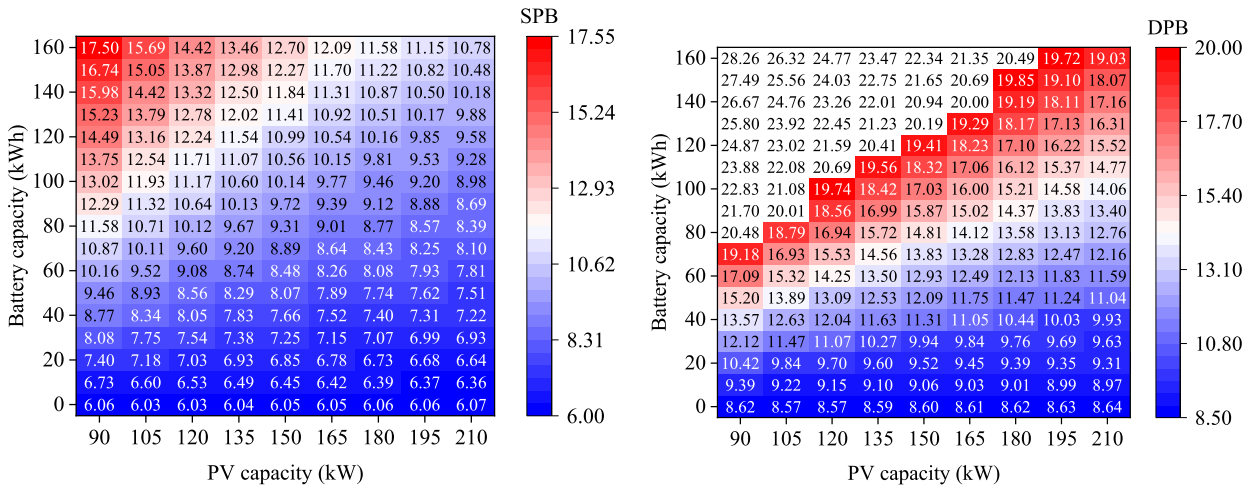

Fig. 16. The payback period of grid-connected PVAC coupling systems with different capacities. (a) SPB (b) DPB.

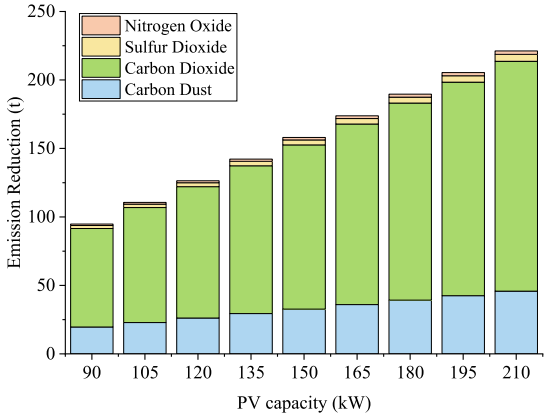

Fig. 17. The environmental performance of PVAC coupling system with different capacities.

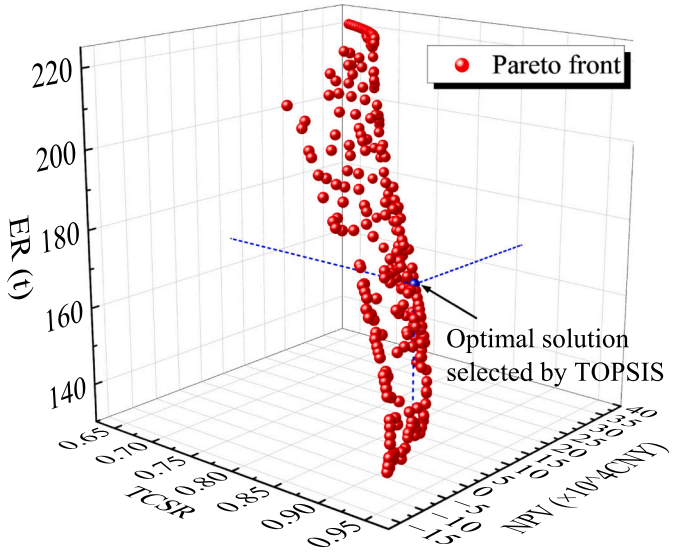

Fig. 18. Pareto front.

capacity design and control strategy. With the initial data and parameters setting above, the results set of Pareto front could be obtained via the optimization algorithm. The Pareto front of the multi-objective optimization is calculated by NSGA-II method.

4.4.1. Capacity optimization of off-grid PVAC coupling system

In the PVAC system coupled with load flexibility and batteries, the optimization objectives are TCSR, NPV, and ER. Based on the three objectives, the result set is presented in Fig. 18. Fig. 19 (a), (b), (c) shows the top view, left view, and right view of Fig. 18. During the optimization process, the TCSR spans from 65.43 % to 93.92 %, the NPV ranges from −106,300 to 359,600 CNY, and the ER varies from 134.91 tons to 221.21 tons. As illustrated in Fig. 19, an upward trend in TCSR was accompanied by a decline in both the system's economic performance and its emission reduction potential. In the context of ER and NPV, the Pareto front exhibited a relatively uniform distribution within a rectangular domain. The optimal solution selected based on Pareto front is shown in Table 7.

As shown in Table 7, the optimal solution of NSGA-II based on the equal preference of three objective functions is obtained. Besides the single objective function driven based on the result of Pareto front is obtained as well, on the solution of TCSR driven, the TCSR is the highest in the Pareto front, enhancing 8.77 % than the optimal solution, but the performance of economy and pollution reduction is the worst. The solution of NPV driven has the best economic performance, but the TCSR value is 20.08 % smaller than the optimal solution. Lastly, the solution of ER driven produces the smallest emissions, sacrificing the economic and energy performance of the PVAC coupling system.

4.4.2. Capacity optimization of grid-connected PVAC coupling system

Based on the three objectives (GP_{total}, NPV, and ER), the result set is presented in Fig. 20. Fig. 21 (a), (b), (c) depicts the top view, left view, and right view of Fig. 21. During the optimization process, the GP_{total} spans from 381.56 kW to 3578.77 kW, the NPV ranges from −147,000 to 373,400 CNY, and the ER varies from 110.34 tons to 221.21 tons. As shown in Fig. 21, the Pareto fronts of ER and NPV, as well as GP_{total} and NPV, are nearly uniformly distributed within a rectangular plane. There are no distinct positive or negative correlations between these pairs. From Fig. 21 (c), there is a significant correlation between GP_{total} and ER. As the ER value increases, the impact on the utility grid intensifies. The main reason is that the values of GP_{total} and ER are positively correlated with PV capacity. A higher PV capacity results in a larger ER value, which in turn leads to a more substantial impact on the utility grid. The optimal solution selected based on Pareto front is shown in Table 8. As shown in Table 8, the solution of NPV driven has the best economic performance, but the GP_{total} is 1779 kW larger than the optimal solution. For the solution of ER driven, it produces the smallest emissions, sacrificing the energy performance of the PVAC coupling

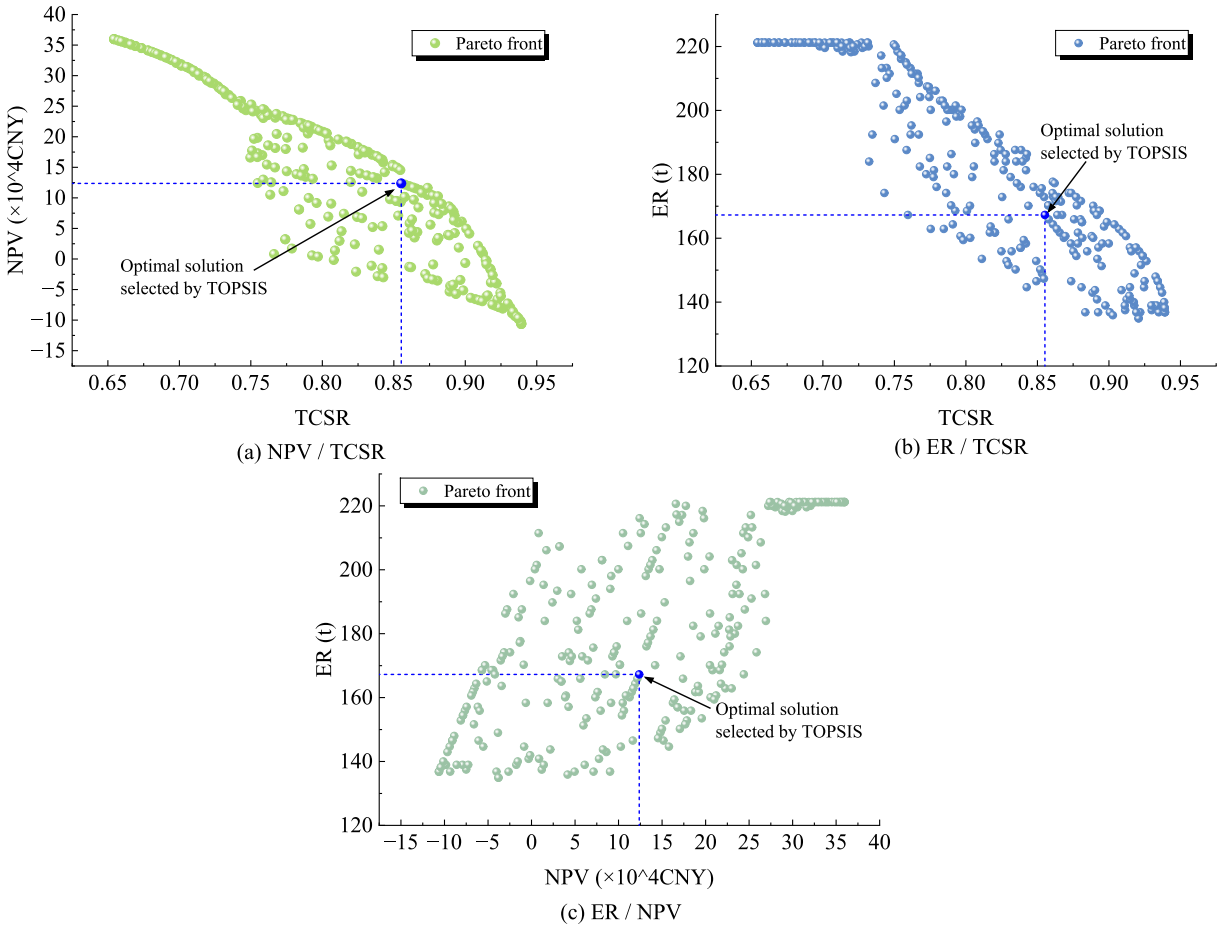

Fig. 19. Top, Left, and Right view of Pareto front.

Table 7
Optimal solutions based on Pareto front.

	PV capacity (kW)	Battery capacity (kWh)	TCSR (%)	NPV ($\times 10^4$CNY)	ER (ton)
TCSR driven	120	160	94.29	−12.34	126.41
NPV driven	210	0	64.69	35.66	221.21
ER driven	210	0	64.69	35.66	221.21
Optimal solution	158.79	74.1	85.52	12.38	167.26

system. The optimal solution has a great performance covering energy matching, economics, and pollution emissions, which can reduce GP_{total} by 1779 kW. This study provides capacity design methodologies and control strategies to achieve multi-objective optimization of PVAC systems, offering implementation guidance for grid-tied solar photovoltaic applications.

5. Conclusions

The PV driven air conditioning system integrated with load flexibility, batteries, and grid interaction offer a viable pathway to achieve zero-energy and carbon-neutral buildings. This research has developed a hierarchical multi-objective co-optimization framework for capacity design and control strategy of PVAC systems considering energy, economic, and environmental objectives comprehensively. In the framework, a three-stage optimization control strategy of load flexibility, batteries and utility grids was proposed based on spatial-temporal

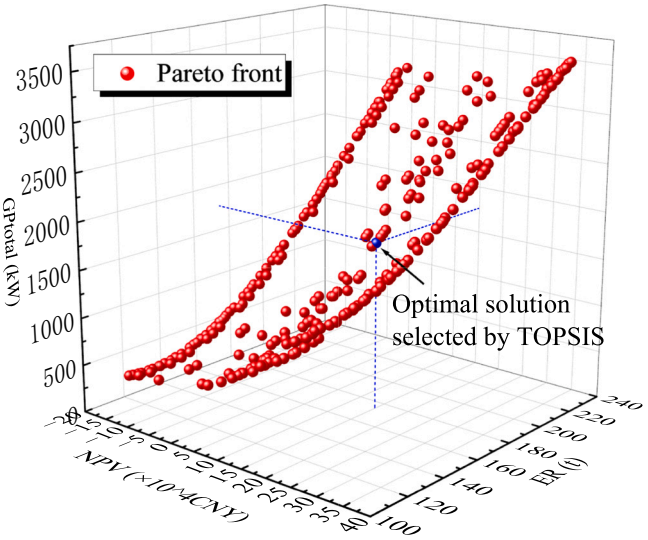

Fig. 20. Pareto front for grid-connected PVAC coupling systems.

occupancy features and thermal comfort and different grid interaction mechanisms. The multi-objective optimized capacities of PV and batteries was obtained by integrating Non-dominated Sorting Genetic Algorithm (NSGA-II). The key conclusions are as follows:

(1) A three-stage control strategy based on spatial-temporal occupancy features was developed to enhance real-time energy

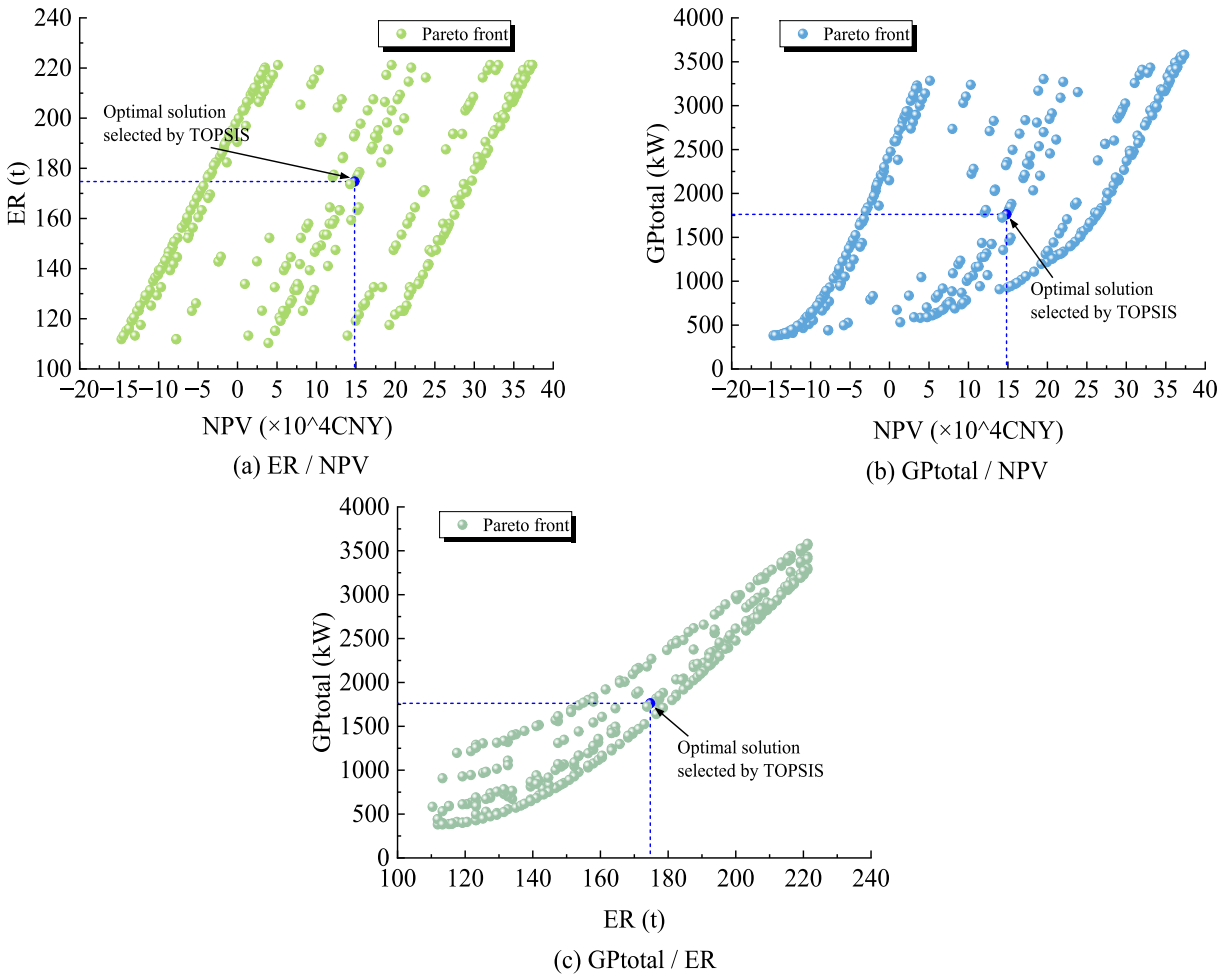

Fig. 21. Top, Left, and Right view of Pareto front.

Table 8
Optimal solutions for grid-connected PVAC coupling systems.

	PV capacity (kW)	Battery capacity (kWh)	NPV (×104CNY)	ER (ton)	GP_{total} (kW)
NPV driven	210	0	37.05	221.21	3640.8
ER driven	210	0	37.05	221.21	3640.8
GPtotal driven	105	160	−14.93	110.61	286.6
Optimal solution	165.88	71.26	14.83	174.7	1861.8

matching. By dynamically adjusting cooling distribution across offices, meeting rooms, and classrooms according to occupant behavior patterns and thermal comfort ranges, the strategy reduces required PV capacity by 24 % while maintaining 85.52 % TCSR. This strategy mitigates energy mismatches caused by insufficient utilization of load flexibility and reduces the reliance on oversized batteries or excessive grid interactions.

(2) A unified 3E (energy-economic-environmental) evaluation method was established to balance conflicting objectives during optimization process. Specifically, a 10 % improvement in TCSR necessitates a 25,000 CNY battery investment while achieving 12 tons of emission reductions. For off-grid systems, the optimized configuration attained 85.52 % TCSR with 123,800 CNY of NPV and 167.26 tons of ER. For grid-connected systems, the optimized system achieved 1861.8 kW of GP_{total} with 148,300 CNY of NPV and 174.70 tons of ER. This evaluation method provides a systematic approach to balance energy matching, economic feasibility, and environmental performance throughout PVAC system implementation.

(3) A hierarchical multi-objective co-optimization framework was proposed for capacity design and control strategy of PVAC coupling systems. For off-grid systems, the optimized PV capacity and battery capacity are 158.79 kW and 74.1 kWh. For grid-connected systems, the corresponding capacities are 165.88 kW and 71.26 kWh. The proposed methodology provides a practical tool for zero-energy building design and energy control by systematically addressing conflicting objectives.

In our future work, the research will be extended in three directions. Firstly, scaling to building clusters will be achieved through the exploration of collaborative optimization mechanisms for multi-building PVAC systems, which incorporate inter-building energy sharing and load interaction. Secondly, grid demand response strategies will be integrated to investigate dynamic scheduling of PV generation, battery storage, and flexible AC loads in response to real-time electricity prices and grid load signals. Thirdly, building envelope parameters (e.g., heat transfer characteristics, window-wall ratio, orientation) will be optimized to minimize cooling loads and improve PV-load matching for integrated net-zero solutions.

Abbreviations

3E	Energy, economic, and environmental	SOC	State of charge
		SPB	Static payback period
AC	Air conditioner	SS	Self-sufficiency
CNY	Chinese Yuan	TCSR	Thermal comfort satisfaction ratio
COP	Coefficient of performance	TCTR	Thermal comfort temperature range
DPB	Dynamic payback period	TOPSIS	Technique for Order Preference by Similarity to an Ideal Solution
ER	Emission reduction		
GP	Grid action power	XGBoost	Extreme Gradient Boosting
HVAC	Heating, ventilation, and air conditioning	ZEBs	Zero energy buildings
LCOE	Levelized cost of energy	***Subscripts***	
MOO	Multi-objective optimization	AC	Air conditioner
NPV	Net present value	b	Battery
NSGA-II	Non-dominated sorting genetic algorithm-II	ch	Charging
PB	Payback period	dis	Discharging
PCM	Phase change materials	g	Grid
PTPS	Part time part space	PV	Photovoltaic
PV	Photovoltaic	***Nomenclatures***	
PVAC	Photovoltaic driven air conditioner	η	Efficiency (%)
RZEP	Real-time zero energy probability	m	Mass (kg)
SC	Self-consumption	obj	Objective functions
SF	Solar factor	P	Power (kW)

CRediT authorship contribution statement

Sihui Li: Writing – review & editing, Validation, Funding acquisition, Formal analysis, Conceptualization. **Yonghuan Li:** Writing – original draft, Software, Methodology, Formal analysis. **Meng Wang:** Writing – review & editing, Funding acquisition. **Li Xie:** Software, Formal analysis. **Guowei Bo:** Writing – review & editing. **Chujie Lu:** Formal analysis.

Declaration of competing interest

The authors declare that they have no known competing financial interests or personal relationships that could have appeared to influence the work reported in this paper.

Acknowledgments

This work was supported by the National Natural Science Foundation of China (Grant No. 52408100 and No. 52108070), the Natural Science Foundation of Hunan Province (Grant No. 2023JJ40038 and No. 2025JJ50285).

Data availability

Data will be made available on request.

References

[1] K.A. Ali, M.I. Ahmad, Y. Yusup, Issues, impacts, and mitigations of carbon dioxide emissions in the building sector, Sustainability 12 (18) (2020) 7427.
[2] Y. Zhu, Y. He, Q. Zhou, Impact of multi-energy complementary system on carbon emissions: Insights from a rural building in Shangluo City, China, Energy Convers. Manag. 327 (2025) 119595.
[3] Y. Cao, N. Zhang, X. Zhang, et al., Comprehensive design and 3E analysis of an ORC-based waste heat recovery system with multiple waste heat feeds from ammonia production, Energy Convers. Manag. 327 (2025) 119597.
[4] Q. Dong, K. Xing, H. Zhang, Artificial neural network for assessment of energy consumption and cost for cross laminated timber office building in severe cold regions, Sustainability 10 (1) (2017) 84.
[5] N. Hussein, A. Al Jubori, A. Abdul-Zahra, Enhancing the performance of air conditioning systems by integrating phase change materials: A comprehensive review, J Energy Storage 101 (2024) 113857.
[6] C. Chang, M. Fang, Impact of a sharing economy and green energy on achieving sustainable economic development: Evidence from a novel NARDL model, J. Innov. Knowl. 8 (1) (2023) 100297.
[7] Munusamy, A., Barik, D., Sharma, P et al Experimental and CFD analysis of dimple tube parabolic trough solar water heater with various nanofluids[J]. Appl. Nanosci., 14(2): 291-337 (2024).
[8] Munusamy, A., Barik, D., Sharma, P. et al Performance analysis of parabolic type solar water heater by using copper-dimpled tube with aluminum coating[J]. Environ. Sci. Pollut. Res., 2024, 31(44): 62376-62391.
[9] H. Li, J. Li, S. Li, et al., Matching characteristics and AC performance of the photovoltaic-driven air conditioning system, Energy 264 (2023) 126509.
[10] Q. Li, Y. Zhou, F. Wei, et al., Harmonizing comfort and energy: A multi-objective framework for central air conditioning systems, Energy Convers. Manag. 314 (2024) 118651.
[11] Nasser, M, Al-Dossari, M, Abd EL-Gawaad, N S, et al . Towards net-zero carbon cooling: A comprehensive study on PCM-integrated condenser and green hydrogen power supply in air conditioning systems[J]. J Energy Storage, 2025, 114:115790.
[12] A. Adeyemo, O. Amusan, Modelling and multi-objective optimization of hybrid energy storage solution for photovoltaic powered off-grid net zero energy building, J Energy Storage 55 (2022) 105273.
[13] V. Nguyen, P. Sharma, B. Bora, et al., Techno-economic analysis of a hybrid energy system for electrification using an off - grid solar/biogas/battery system employing HOMER: A case study in Vietnam, Process. Saf. Environ. Prot. 191 (2024) 1353–1367.
[14] K. Wang, J. Peng, S. Li, et al., Compressor speed control for optimizing energy matching of PV-driven AC systems during the cooling season, Energy 298 (2024) 131270.
[15] H. Xu, L. Cheng, N. Qi, et al., Peak shaving potential analysis of distributed load virtual power plants, Energy Rep. 6 (2020) 515–525.
[16] R.S. Alshareef, H.M. Maghrabie, Building-integrated photovoltaics with energy storage systems–A comprehensive review, J Energy Storage 116 (2025) 115916.
[17] Y. Chen, Y. Liu, J. Liu, et al., Design and adaptability of photovoltaic air conditioning system based on office buildings, Sol. Energy 202 (2020) 17–24.
[18] J. Zhao, Z. Yang, L. Shi, et al., Photovoltaic capacity dynamic tracking model predictive control strategy of air-conditioning systems with consideration of flexible loads, Appl. Energy 356 (2024) 122430.
[19] S. Li, J. Peng, B. Zou, et al., Zero energy potential of photovoltaic direct-driven air conditioners with considering the load flexibility of air conditioners, Appl. Energy 304 (2021) 117821.
[20] S. Li, J. Peng, H. Li, et al., Zero energy potential of PV direct-driven air conditioners coupled with phase change materials and load flexibility, Renew. Energy 200 (2022) 419–432.
[21] M. Aneke, M. Wang, Energy storage technologies and real life applications–a state of the art review, Appl. Energy 179 (2016) 350–377.
[23] R. Opoku, K. Mensah-Darkwa, A.S. Muntaka, Techno-economic analysis of a hybrid solar PV-grid powered air-conditioner for daytime office use in hot humid climates–a case study in Kumasi city, Ghana, Sol. Energy 165 (2018) 65–74.
[24] H. Ozcan, S. Varga, H. Gunerhan, et al., Numerical simulation and parametric study of various operational factors affecting a PV-battery-air conditioner system under prevailing European weather conditions, Sustain. Cities Soc. 67 (2021) 102754.
[25] Schram, W, Lampropoulos, I, Wilfried, G, et al . Photovoltaic systems coupled with batteries that are optimally sized for household self-consumption: Assessment of peak shaving potential[J]. Appl. Energy, 2018, 223: 69-81.
[26] A.O.M. Maka, T.N. Chaudhary, Performance investigation of solar photovoltaic systems integrated with battery energy storage, J Energy Storage 84 (2024) 110784.
[27] S. Li, J. Peng, Y. Tan, et al., Study of the application potential of photovoltaic direct-driven air conditioners in different climate zones, Energy Build. 226 (2020) 110387.
[28] K. Wang, J. Peng, S. Li, et al., Compressor speed control for optimizing energy matching of PV-driven AC systems during the cooling season, Energy 298 (2024) 131270.
[29] H. Ren, Y. Sun, A. Albdoor, et al., Improving energy flexibility of a net-zero energy house using a solar-assisted air conditioning system with thermal energy storage and demand-side management, Appl. Energy 285 (2021) 116433.
[30] J. Salpakari, P. Lund, Optimal and rule-based control strategies for energy flexibility in buildings with PV, Appl. Energy 161 (2016) 425–436.
[31] S. Guo, F. Ren, Z. Wei, et al., A multi-objective collaborative planning method for a PV-powered hybrid energy system considering source-load matching, Energy Convers. Manag. 316 (2024) 118848.
[32] J. Jung, D. Kim, Y. Jung, et al., A novel control strategy for optimizing combined cooling, heating, and power systems with energy storage devices in commercial buildings, Energy Convers. Manag. 326 (2025) 119517.
[33] M. Kahsay, S. Voller, Thermal energy storage for increasing self-consumption of grid connected photovoltaic systems: A case for Skjetlein High School, Norway, Energy Build. 335 (2025) 115563.
[34] Z. Wang, M. Luther, P. Horan, et al., On-site solar PV generation and use: Self-consumption and self-sufficiency, Build. Simul. 16 (2023) 1835–1849.
[35] Y. Li, B. Zhao, Z. Zhao, et al., Performance study of a grid-connected photovoltaic powered central air conditioner in the South China climate, Renew. Energy 126 (2018) 1113–1125.

[36] E.M. Salilih, Y.T. Birhane, Modeling and performance analysis of directly coupled vapor compression solar refrigeration system, Sol. Energy 190 (2019) 228–238.
[37] B. Zou, Y. Lei, J. Peng, et al., Improving the real-time energy matching performance of PV-based home energy system: A multi-time resolution scheduling method utilizing flexibility of thermostatically controlled loads and batteries, Energy Build. 328 (2025) 115158.
[38] F. Eze, J. Ogola, R. Kivindu, et al., Technical and economic feasibility assessment of hybrid renewable energy system at Kenyan institutional building: A case study, Sustain Energy Technol Assess 51 (2022) 101939.
[39] A. Al-Ugla, M. El-Shaarawi, S. Said, et al., Techno-economic analysis of solar-assisted air-conditioning systems for commercial buildings in Saudi Arabia, Renew. Sust. Energ. Rev. 54 (2016) 1301–1310.
[40] W. Herche, Solar energy strategies in the U.S. utility market, Renew. Sust. Energ. Rev. 77 (2017) 590–595.
[41] M. Mahmoudi, M. Dehghan, H. Haghgou, et al., Techno-economic performance of photovoltaic-powered air-conditioning heat pumps with variable-speed and fixed-speed compression systems, Sustain Energy Technol Assess 45 (2021) 101113.
[42] A. Sohani, A. Dehnavi, H. Sayyaadi, et al., The real-time dynamic multi-objective optimization of a building integrated photovoltaic thermal (BIPV/T) system enhanced by phase change materials, J Energy Storage 46 (2022) 103777.
[43] F. Aguilar, D. Crespí-Llorens, P. Quiles, Techno-economic analysis of an air conditioning heat pump powered by photovoltaic panels and the grid, Sol. Energy 180 (2019) 169–179.
[44] Leite, L, Weschenfelder, F, Araújo, A, et al . An economic analysis of the integration between air-conditioning and solar photovoltaic systems[J]. Energy Convers. Manag., 2019, 185:836-849.
[45] L. Wang, T. Qiu, M. Zhang, et al., Carbon emissions and reduction performance of photovoltaic systems in China, Renew. Sust. Energ. Rev. 200 (2024) 114603.
[46] Aguilar, F J, Ruiz, J, Lucas, M et al Performance analysis and optimization of a solar on-grid air conditioner[J]. Energies, 2021, 14(23): 8054.
[47] R. Wang, S. Hasanefendic, E. Von Hauff, et al., Towards carbon neutrality: A multi-objective optimization model for photovoltaics systems installation planning, Sustain Energy Technol Assess 62 (2024) 103625.
[48] A. Albatayneh, M. Jaradat, M. Al-Omary, et al., Evaluation of coupling PV and air conditioning vs. solar cooling systems—case study from Jordan, Appl. Sci. 11 (2) (2021) 511.
[49] G. Li, Y. Han, M. Li, et al., Study on matching characteristics of photovoltaic disturbance and refrigeration compressor in solar photovoltaic direct-drive air conditioning system, Renew. Energy 172 (2021) 1145–1153.
[50] T. Samarasinghalage, W. Wijeratne, R. Yang, et al., A multi-objective optimization framework for building-integrated PV envelope design balancing energy and cost, J. Clean. Prod. 342 (2022) 130930.
[51] B.Y. Zhao, Y. Li, R.Z. Wang, et al., A universal method for performance evaluation of solar photovoltaic air-conditioner, Sol. Energy 172 (2018) 58–68.
[52] B.J. Huang, T.F. Hou, P.C. Hsu, et al., Design of direct solar PV driven air conditioner, Renew. Energy 88 (2016) 95–101.
[53] S. Loem, A. Asanakham, T. Deethayat, et al., Testing of solar inverter air conditioner with PCM cool storage and sizing of photovoltaic modules, Thermal Science and Engineering Progress 38 (2023) 101671.
[54] Y. Chen, Y. Liu, Y. Wang, et al., The research on solar photovoltaic direct-driven air conditioning system in hot-humid regions, Procedia Engineering 205 (2017) 1523–1528.
[55] F.J. Aguilar, J. Ruiz, M. Lucas, et al., Performance analysis and optimisation of a solar on-grid air conditioner, Energies 14 (23) (2021) 8054.
[56] X. Su, C. Luo, J. Ji, et al., Assessment of photovoltaic performance and carbon emission reduction potential of bifacial PV systems for regional grids in China, Sol. Energy 269 (2024) 112367.
[57] M. Wang, X. Mao, Y. Gao, et al., Potential of carbon emission reduction and financial feasibility of urban rooftop photovoltaic power generation in Beijing, J. Clean. Prod. 203 (2018) 1119–1131.
[58] L. Wan, B. Zou, J. Peng, et al., Multi-objective hierarchical co-optimization of battery capacity configuration and operational strategy for photovoltaic-battery systems in buildings, J Energy Storage 114 (2025).
[59] Alomar, O R, Basher, N M, Ali, O M, et al . Energetic, economic environmental analysis for photovoltaic grid-connected systems under different climate conditions in Iraq[J]. Cleaner Energy Systems, 2025, 10.